Original article

# Strategy for cysteine-targeting covalent inhibitors screening using in-house database based LC-MS/MS and drug repurposing

Xiaolan Hu [a, b], Jian-Lin Wu [a, **], Quan He [a], Zhi-Qi Xiong [c], Na Li [a, *]

[a] State Key Laboratory of Quality Research in Chinese Medicine, Macau University of Science and Technology, Taipa, Macau SAR, 999078, China
[b] College of Environment and Climate, Institute of Mass Spectrometry and Atmospheric Environment, Guangdong Provincial Key Laboratory of Speed Capability Research, Jinan University, Guangzhou, 510632, China
[c] Center for Excellence in Brain Science and Intelligence Technology, Institute of Neuroscience and State Key Laboratory of Neuroscience, Chinese Academy of Sciences, Shanghai, 200031, China

## ARTICLE INFO

## ABSTRACT

Targeted covalent inhibitors, primarily targeting cysteine residues, have attracted great attention as potential drug candidates due to good potency and prolonged duration of action. However, their discovery is challenging. In this research, a database-assisted liquid chromatography-tandem mass spectrometry (LC-MS/MS) strategy was developed to quickly discover potential cysteine-targeting compounds. First, compounds with potential reactive groups were selected and incubated with N-acetyl-cysteine in microsomes. And the precursor ions of possible cysteine-adducts were predicted based on covalent binding mechanisms to establish in-house database. Second, substrate-independent product ions produced from N-acetyl-cysteine moiety were selected. Third, multiple reaction monitoring scan was conducted to achieve sensitive screening for cysteine-targeting compounds. This strategy showed broad applicability, and covalent compounds with diverse structures were screened out, offering structural resources for covalent inhibitors development. Moreover, the screened compounds, norketamine and hydroxynorketamine, could modify synaptic transmission-related proteins in vivo, indicating their potential as covalent inhibitors. This experimental-based screening strategy provides a quick and reliable guidance for the design and discovery of covalent inhibitors.

## 1. Introduction

Targeted covalent inhibitors have capture growing interest as potential drug candidates due to their benefits in term of high potency and prolonged duration of action [1,2]. Targeting the nucleophile cysteine residues of protein with electrophilic reactive groups (a "warhead") is the predominant strategy for the development of targeted covalent inhibitor since cysteine is highly intrinsically reactive amino acid, e.g. Food and Drug Administration (FDA)-approved targeted covalent inhibitors sotorasib (KRAS[G12C] inhibitor) [3], ibrutinib (Bruton's tyrosine kinase inhibitor (BTK inhibitor)) [4], and afatinib (epidermal growth factor receptor inhibitor (EGFR inhibitor)) [5]. The covalent interaction effectively decouples drug pharmacodynamics from pharmacokinetics, allowing for sustained efficacy beyond metabolic clearance [6]. The

advantage brought by this unique feature of covalent inhibitors is reduced dosage and frequency of administration, improving medication compliance [7]. Therefore, the investigation of cysteine-targeting compounds is of great significance for the design and discovery of covalent inhibitors.

Recently, a host of approaches have emerged for the development of covalent cysteine inhibitors. Large-scale structure-based covalent virtual screening has been employed for covalent inhibitors discovery [8]. While successful, structure-based computational method tends to produce a large number of false-positive hits, which limit its application as a standalone technique [9,10]. And the methodology is constrained by the extant libraries, thereby restricting the discovery of structurally diverse and novel covalent inhibitors [11]. Furthermore, it cannot assess the intrinsic reactivity of electrophilic molecules [12]. The selectivity and activity of thousands of hit molecules obtained by virtual screening must be confirmed by high-throughput screening. Unfortunately, high-throughput screening for hit compounds can be plagued by false positives resulting from non-specific modifications and promiscuous activity [13]. Fragment-based drug discovery, which

generates compounds from smaller and less complex molecules, has emerged as a complementary approach to high-throughput screening for early-stage drug development. This approach has led to the successful development of several approved drugs [14]. A limitation of fragment-based screening technology is the requirement for greater sensitivity assays coupled with elaborate validation, owing to the weak binding affinity of small molecules to protein targets. Currently, activity-based protein profiling (ABPP) as reactive-cysteine profiling method has been widely used for covalent inhibitor discovery [15,16]. However, the complexity of probe synthesis limits the use of this technique. In addition, ABPP assays are proteomic-level screening techniques that require powerful mass spectrometry (MS) instrument, and the complex sample preparation results in their relatively low throughput. Therefore, a simple and rapid screening approach for cysteine-targeting compound is urgently needed for covalent drug development.

It is worth noting that many early covalent drugs are discovered serendipitously, which are found to act through covalent mechanisms after being approved for use via non-covalent interactions, such as aspirin [17]. Thus, considering the slow pace and substantial costs of new drug development, repurposing of existing drugs is an attractive strategy to provide an effective opportunity for covalent drugs discovery because it involves the use of de-risked compounds [18]. It has been well known that drugs containing electrophilic reactive groups, such as acrylamide, epoxide, and α,β-unsaturated carbonyl, can directly react with nucleophilic cysteine residues [7,19]. In addition, some drugs can be biotransformed into electrophilic reactive metabolites by enzymes to covalently bind to cysteine residues. For example, the demethylated metabolite of osimertinib, AZ5104, has been reported to covalently attach to cysteine residues of its functional target protein, EGFR, and to be more potent than the prototype drug in so doing [20,21]. Therefore, the modification patterns, either compound *per se* or its metabolites, have the potential to be developed as covalent drugs. Moreover, the mere presence of electrophilic reactive groups does not indicate that the compound could covalently bind to cysteine residues because the covalent interactions are dependent on the reactivity of electrophilic reactive groups present in different molecular structures, which need to be demonstrated through experiments.

Currently, MS based strategy, both global profiling and targeted detection, play an important role in the detection and quantitation of multiple metabolites from various specimen [22,23]. In particular, multiple reaction monitoring (MRM) by liquid chromatography triple quadrupole (LC-QQQ) mass spectrometer is a highly sensitive approach that enables highly selective measurement of the target compounds based on the appropriate precursor-product ion pairs, thereby reducing the interference of overlapping peaks. Therefore, MS methods for faster discovery of cysteine-targeting compounds present an attractive prospect to improve the efficiency of exploratory covalent drugs.

In this study, we proposed a database-assisted liquid chromatography-tandem mass spectrometry (LC-MS/MS) strategy for potential cysteine-targeting compounds screening. This strategy was validated to be efficient and sensitive for the detection of potential cysteine-targeting compounds prior to structural elucidation. Using this strategy, 17 novel cysteine-targeting compounds or metabolites were screened, providing candidates for covalent drugs development. Moreover, the potential candidates have been validated at proteome level *in vitro*. Furthermore, two novel covalent inhibitors candidates and their associated modified proteins have been discovered *in vivo* for the treatment of long-term depression.

## 2. Materials and methods

### 2.1. Chemicals and materials

Triptolide (TP, purity >99%), celastrol (CE, purity >98%), and ibrutinib (PCI, purity >99%) were supplied by Chengdu Mansite Pharmacetical Co., Ltd. (Chengdu, China). Resibufogenin (RES, purity >99%), naringenin (NAR, purity >93%), and ciprofloxacin (CIP, purity >98%) were purchased from J&K (Beijing, China). Osimertinib (AZD, purity >98%) was purchased from AbMole BioScience Inc (Houston, TX, USA). Ozenoxacin (OZE, purity >98%) was purchased from AmBeed Inc (Arlington Heights, IL, USA). Ketamine hydrochloride (KET) was obtained from the Institute of Neuroscience, Chinese Academy of Sciences (Shanghai, China). Sunitinib (SU, purity >98%), *N*-acetyl cysteine (NAC), urea, ammonium bicarbonate, ammonium acetate, and trifluoroacetic acid (TFA) were purchased from Sigma-Aldrich (St. Louis, MO, USA). Pooled human liver microsomes (HLMs) and nicotinamide adenine dinucleotide phosphate (NADPH) generating solutions A and B were obtained from BD Gentest (San Jose, CA, USA). Bovine serum albumin (BSA) was obtained from Affymetrix (Santa Clara, CA, USA). Dithiothreitol (DTT), and iodoacetamide (IAA) were purchased from GE Healthcare (Piscataway, NJ, USA). Trypsin protease (MS grade) was obtained from Thermo Fisher Scientific (Rockford, IL, USA). BIO-RAD DC Protein Assay Reagent was purchased from Bio-Rad (Richmond, CA, USA). The solid-phase extraction (SPE) $C_{18}$ cartridge was provided from Waters Corporation (Milford, MA, USA). MS grade acetonitrile (ACN) was purchased from Anaqua Chemicals Supply Inc. Ltd. (Houston, TX, USA). Deionized water was prepared using a Milli-Q® system (Millipore Corporation, Billerica, MA, USA).

### 2.2. Establishment of the in-house database

Based on the literature of phase I and II metabolites of compounds, Human Metabolome Database (HMDB), and Bio-Transformer 3.0, the possible metabolites of compounds were predicted. Then, the potential NAC adducts formed with compounds or their metabolites were hypothesized based on the covalent binding mechanism to establish an in-house NAC adducts database.

### 2.3. Incubation of compounds and NAC in microsomes

The compounds were dissolved in methanol at a concentration of 1 mg/mL. Compound (50 μM) was incubated with NAC (5.0 mM) in the presence of microsomes (1.0 mg/mL) and NADPH-generating system solutions A and B in potassium phosphate buffer (PBS, 0.1 M, pH 7.4) at 37 °C. The total incubation volume was 200 μL. And then the metabolic reactions were terminated by quenching with five volumes of ice-cold ACN at 240 min. After vortex-mixed and centrifuged at 15,000 *g* for 10 min at 4 °C, the resulting supernatants were collected and evaporated to dryness under a nitrogen stream. The residues were reconstituted with 50 μL of 50% methanol in water and centrifuged prior to LC-MS analysis. The reactions of NAC in microsomes without compounds were also conducted in parallel.

### 2.4. Multiple reaction monitoring (MRM) screening for potential cysteine-targeting covalent compounds

The MRM screening was conducted on an Agilent ultra-high-performance coupled with triple quadrupole mass spectrometry (UHPLC-QQQ-MS) system. Agilent 1290 infinity UHPLC (Agilent Technologies, Santa Clara, CA, USA) with binary pump equipped

with Waters ACQUITY UPLC BEH $C_{18}$ column (2.1 mm $\times$ 100 mm, 1.7 μm; Waters, Milford, MA, USA) was employed for the separation of components. The flow rate was 0.25 mL/min. The mobile phase consisted of 0.1% (v/v) formic acid (A) and 0.1% (v/v) formic acid in ACN (B) with the following gradient: 0−0.5min, 5% B; 0.5−2 min, 5%−20% B; 2−4 min, 20%−30% B; 4−6 min, 30%−50% B; 6−8 min, 50%−80% B; 8−10 min, 80%−95% B; 10−11.5 min, 95% B; and 11.5−12 min, 95%−5% B. The injection volume was 1 μL. An Agilent 6490 iFunnel QQQ-MS (Agilent Technologies) with a dual jet stream electrospray ion source (dual AJS ESI) was applied for the screening of NAC adducts. MRM in positive mode was utilized and three characteristic product ions of $m/z$ 130.0, 162.0, and 164.0 were set. The collision cell energy (CE) was set at 35 V, and the signal-to-noise ratio (S/N) was higher than 3. Other MS parameters were optimized and set as follows: gas flow at 13 L/min, gas temperature at 225 °C, sheath gas flow at 12 L/min, sheath gas temperature at 275 °C, nebulizer pressure at 25 psig, nozzle voltage at 350 V, and capillary at 4000 V.

An Agilent 6545 UHPLC-quadrupole time-of-flight (Q-TOF) MS system (Agilent Technologies) was used for the identification of chemicals-cysteine conjugates. The chromatographic conditions were same with that of UHPLC-QQQ-MS. The mass spectrum was acquired in positive ion mode.

### 2.5. Incubation of ketamine and model protein in microsomes

BSA (1 mg/mL) was incubated with ketamine (45.6 μM) in microsomal system (1.0 mg/mL) including NADPH-generating solutions A and B for 120 min at 37 °C. After centrifugation at 10,000 $g$ for 5 min, the supernatants were collected and mixed with 4 times volumes of cold acetone. The precipitates were collected and redissolved in urea (8 M) followed by centrifugation at 10,000 $g$ for 5 min at 4 °C. The protein concentrations were quantified by Bio-Rad DC Protein Assay Reagent. The control samples without ketamine were also prepared in parallel. Samples were prepared in triplicate.

### 2.6. Animal care and drug treatment

Eight-week male C57BL/6 J mice (Vital River, Beijing, China) were housed in 12 h light/dark cycles in a temperature-controlled room and given *ad libitum* access to food and water. All experimental procedures were performed in accordance with all institutional guidelines and ethics and approved by the Animal Use and Care Committee of the Center for Excellence in Brain Science and Intelligence Technology (Institute of Neuroscience), Chinese Academy of Sciences (Approve No.: NA-009-2019).

The mice were randomly divided into four groups ($n = 3$ for each group). Mice in groups 1, 2 and 3 were given a single intraperitoneal (i.p.) injection of 30 mg/kg ketamine, respectively, while the control group was given a single i. p. injection of saline. The animals in each group were anesthetized with a nembutal sodium solution (50 mg/kg of body weight). Mice were sacrificed by decapitation. Then the whole brain from all groups were dissected out, and the hippocampus were separated on ice. All samples were frozen in liquid nitrogen and stored at −80 °C before analysis.

### 2.7. Digestion of protein samples

Mice hippocampal samples were homogenized with 10 vol (w/v) phosphate buffer (pH 7.4). After centrifugation at 9,000 $g$ for 10 min at 4 °C, the supernatants were collected and mixed with 4 vol of ice-cold acetone. The mixture was processed by centrifugation at 10,000 $g$ for 5 min at 4 °C. After washed twice with ice-cold acetone, the supernatants were collected and subjected to UHPLC-Q-TOF-MS analysis. And the precipitates were digested with trypsin according to our previous reports [24,25]. The proteins (100 μg) were diluted with water to a final concentration of 1 mg/mL and then reduced with DTT (200 mM) for 60 min at room temperature, and then alkylated in IAA (1 M) for 60 min in the dark. The reaction mixture was quenched with DTT (200 mM) for 60 min at room temperature. The mixture was diluted with 25 mM bicarbonate until the concentration of urea was below 1 M. Finally, the proteins were digested with trypsin at 37 °C overnight with an enzyme/protein ratio of 1:50 (w/w). The peptides digests were desalted using SPE $C_{18}$ cartridge, and the elution was dried under nitrogen. The residues were reconstituted with 2% acetonitrile containing 0.1% TFA in water and centrifuged prior to two-dimensional (2D) strong cation-exchange (SCX)-nano-LC-Q-TOF-MS analysis to search for the adducted proteins in Mascot. The control samples without ketamine administration were also prepared in parallel.

### 2.8. 2D LC-MS method

2D SCX-nano-LC-Q-TOF-MS was applied for proteomics analysis. A Dionex Ultimate 3000 nanoflow HPLC system (Dionex, Sunnyvale, CA, USA) with a Bruker maXis Impact Q-TOF-MS equipped with a Bruker Advance CaptiveSpray ion source (Bruker Daltonics, Billerica, MA, USA) was employed to separate and identify the peptides. The peptides digestion (30 μg) was injected and loaded onto a strong cation exchange column (Poros 10S, 0.3 mm $\times$ 100 mm; Thermo Scientific) and eluted successively by a series of ammonium acetate with the concentrations of 5, 10, 25, 50, and 100 mM at pH 2.7. Each elution buffer from SCX column was transferred to a $C_{18}$ trap column, and then desalted with solution A (0.1% FA in 2% ACN) at a flow rate of 5 μL/min for 30 min. Then, the desalted fractions were separated in a $C_{18}$ analytical column (50 cm $\times$ 75 μm, Acclaim PepMap RSLC, Thermo Scientific) at a flow rate of 300 nL/min. The chromatographic conditions were the same as our previous public [24].

### 2.9. Identification of modified proteins

The raw data were processed by Bruker Compass Data Analysis software and searching protein database (SwissProt 56.0) by use of Mascot server (version 2.3.0, Matrix Science, London, UK). Four possible ketamine modified molecular compositions, $C_{13}H_{14}ClNO$ (C+235 Da, K1), $C_{12}H_{12}ClNO$ (C+221 Da, K2), $C_{12}H_{12}ClNO_2$ (C+237 Da, K3), and $C_{13}H_{12}ClNO_2$ (C+249 Da, K4) were input into the Mascot server as variable modifications. Carbamidomethyl (C) and methionine oxidation (M) were also selected as variable modifications. Data were searched using the following parameters: the precursor and fragment mass tolerance were set at 30 ppm and 0.2 Da, respectively; peptide charge was 2+, 3+, and 4+; trypsin was selected as the enzyme; maximum missed cleavage was 1 allowed; statistical significance was set at $P < 0.05$, and peptide spectral matches were validated based on q-values to 1% FDR using percolator.

## 3. Results and discussion

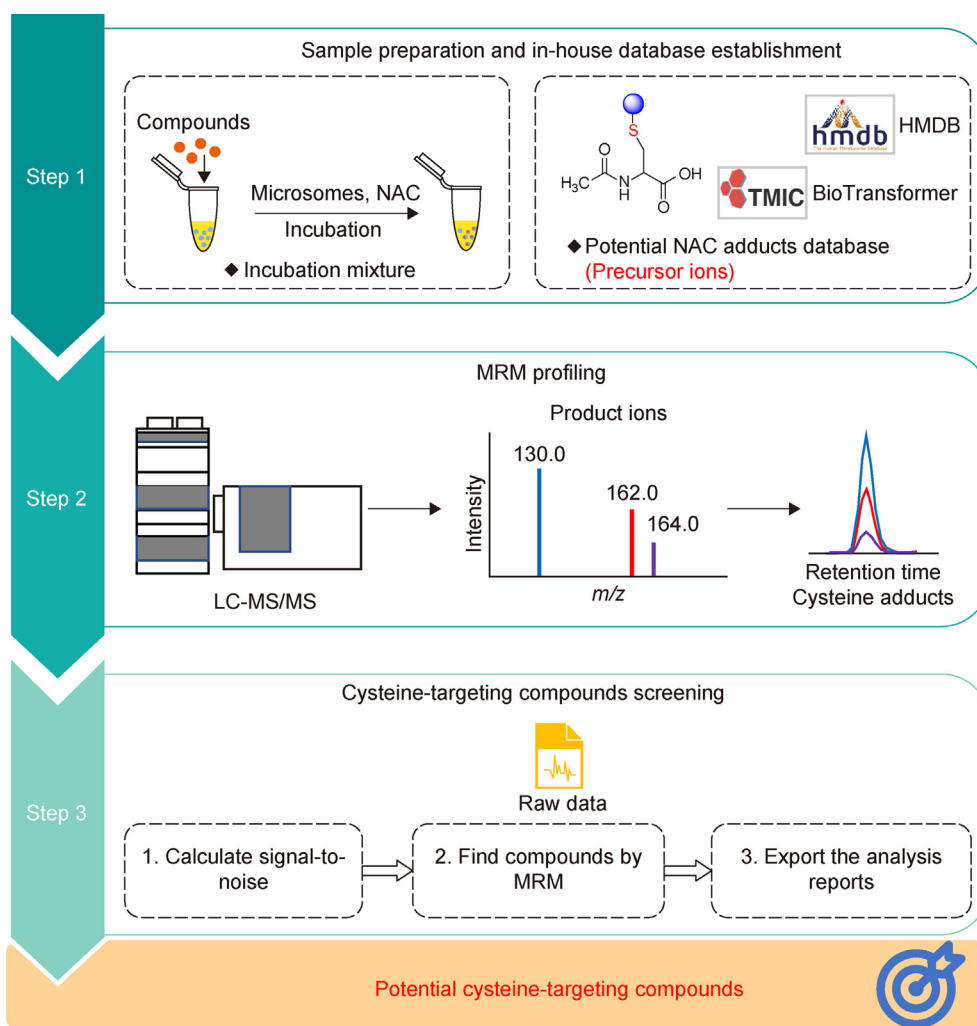### 3.1. New strategy for cysteine-targeted covalent inhibitor screening

To rapidly screen potential covalent inhibitors targeting cysteine residues of proteins, we propose a database-assisted LC-MS/MS strategy based on the covalent binding mechanisms (Fig. 1).

Considering the potential of existing drugs to be repurposed as covalent drugs, compounds with potential electrophilic groups are selected for the study (Table 1). Furthermore, since metabolic activation can also produce electrophilic groups to react with cysteine residues, liver microsomal incubation system is utilized to discover more potential covalent drug candidates. In addition, NAC is used as a trapping reagent to capture electrophilic substances to form stable products for MS analysis.

First, compound is incubated with NAC in liver microsomal system. And a database of potential NAC adducts formed by compound and/or its metabolites is established as follows for the prediction of precursor ions in LC-MS/MS analysis. The first step involves acquiring chemical formulas and structures of metabolites that contained electrophilic groups (warheads). For known metabolites, their structural information could be acquired from literatures and HMDB. For potential unknown metabolites, their structural information can be predicted using BioTransformer with the cytochrome P450 enzyme metabolite prediction module. Then, the possible NAC adducts formed by the reaction of the electrophilic group of the compound and/or its metabolites with the nucleophilic sulfhydryl of NACs are predicted based on the covalent binding mechanisms. For example, epoxide can react with NAC via the second-order nucleophilic substitution ($S_N2$) mechanism, and $\alpha,\beta$-unsaturated carbonyl

can form NAC adduct through Michael addition reaction (Fig. S1) [26]. Although the reaction mechanisms of epoxides and $\alpha,\beta$-unsaturated carbonyl compounds are different, the molecular formula of the resulting NAC adducts is the sum of the molecular formulas of the substrate or its metabolites and NAC. Phenol-containing compounds can be metabolically activated into reactive quinone intermediate to react with NAC through Michael addition reaction (Fig. S1) [6]. Compounds containing phenyl substitution can be metabolized to benzene oxides and hydroquinones, both of which subsequently conjugate with NAC to form NAC adducts (Fig. S1) [27]. The molecular formula of NAC adducts formed by a compound containing phenol or phenyl is 2H less than the sum of the molecular formulas of the substrate or its metabolites and NAC. Finally, all possible NAC adducts are predicted and listed in the in-house database, providing precursor ions ($[M + H]^+$) for LC-MS/MS analysis.
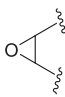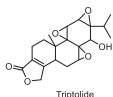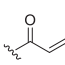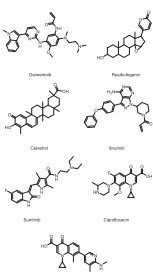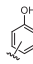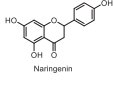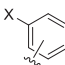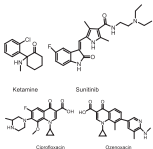
Second, the characteristic product ions of NAC adducts should be selected for MRM scanning. The substrate-independent product ions must be determined to enable high sensitivity and high-throughput screening of NAC adducts. According to our previous investigation, the product ions formed by the cleavage of C-S bond between the substrate and NAC or within NAC are usually produced in the MS/MS spectra of NAC adducts [21,24,25]. Thus, the product ions at $m/z$ 164.0, 162.0, and 130.0 corresponding to the protonated



**Fig. 1.** Flowchart for cysteine-targeting compounds screening. NAC: *N*-acetyl-cysteine; HMDB: Human Metabolome Database; MRM: multiple reaction monitoring; LC-MS/MS: liquid chromatography-tandem mass spectrometry.

**Table 1**
Representative compounds with different potential electrophilic groups and their associated mechanistic domains.

| Electrophilic functional groups | Potentially electrophilic functional groups via bioactivation | Example structure | Compounds | Mechanistic domain |
|---|---|---|---|---|
| Epoxides | |  |  Triptolide | Second-order nucleophilic substitution |
| α,β-unsaturated carbonyls | |  |  Osmertinib, Pseudolaigenin, Celastrol, Ibrutinib, Sunitinib, Ciprofloxacin, Ozenoxacin | Michael addition |
| Phenols | |  |  Naringenin | Michael addition |
| Phenyl | |  |  Ketamine, Sunitinib, Ciprofloxacin, Ozenoxacin | Michael addition |

NAC, S-containing NAC, and NAC with loss of $H_2S$, respectively, should be suitable selections for MRM scanning.

Third, potential NAC adducts would be screened by MRM mode. To simplify and accurately extract the MRM chromatographic peaks of potential NAC adducts, the data analysis workflow is defined by three phases: calculating S/Ns, finding NAC adducts by MRM, and exporting the analysis reports. Alternatively, the detected potential NAC adducts can be verified by LC-high resolution MS system, e.g., UHPLC-Q-TOF-MS/MS.

### 3.2. Strategy validation

Triptolide and osimertinib (Table 1), which contain warheads of epoxide and α,β-unsaturated carbonyl, respectively, are well known to covalently bind with cysteine residues of proteins [21,28]. And naringenin, which contains phenolic groups, is presumed to conjugate with cysteine after bioactivation. These three compounds were chosen as representative compounds with different warheads (Table 1) and covalent binding mechanism to validate above proposed screening strategy. According to previous reports, HMDB database, BioTransformer, and the covalent binding mechanisms, the NAC adducts database was first established (Table 2). The precursor ions and product ions of NAC adducts were imported into LC-MS for positive MRM scan. As a result, 17 peaks were found from the incubation system of these three compounds (Table 2), and each peak represented a potential NAC adduct. Moreover, these adducts were further verified by UHPLC-Q-TOF-MS/MS.

Triptolide is an example of epoxide-containing compounds. Two metabolites of triptolide, a dehydrogenation metabolite and a mono-oxidation metabolite, were obtained from HMDB and Bio-Transformer, and one dehydrated metabolite was reported [29]. All of these metabolites retain epoxide groups. Then four possible

types of NAC conjugates derived from triptolide and its metabolites were predicted based on the $S_N2$ mechanism (Fig. S1), as shown in Table 2. MRM analysis showed five peaks, TC1−TC5 (Fig. 2). The most intense peak of TC1 showed the precursor ion $m/z$ 524.2 and was determined by three MRM transitions (524.2 → 130.0, 524.2 → 162.0, 524.2 → 164.0), corresponding to the triptolide-NAC adduct predicted in the database (Table 2). The accurate mass measurement of protonated molecular ions ($m/z$ 524.1954) of TC1 using Q-TOF gave the chemical formula of $C_{25}H_{33}NO_9S$. And the fragment ions of the NAC moiety at $m/z$ 130.0502, 162.0223 and 164.0381 further confirmed that TC1 was a NAC adduct. In addition, the structure of TC1 was further confirmed by the fragment ions at $m/z$ 395.1518 and 361.1643 produced from the neutral loss of $C_5H_7NO_3$ (−129.0 Da) and NAC (−163.0 Da), respectively (Fig. S2A). A minor chromatographic peak of precursor ion $m/z$ 522.2 (TC2) was determined by two MRM transitions (522.2 → 130.0, 522.2 → 164.0), corresponding to a NAC adduct of dehydrogenated metabolite of triptolide. The protonated molecular ion at $m/z$ 522.1791 with the chemical formula of $C_{25}H_{31}NO_9S$, together with the characteristic NAC fragment ions ($m/z$ 130.0498, and 164.0376), and the fragment ions at $m/z$ 359.1482 ([M + H−NAC]$^+$), 341.1373 ([M + H−NAC−$H_2O$]$^+$) in the Q-TOF-MS/MS spectrum further confirmed the proposed structure of TC2 (Fig. S2B). Other two minor chromatographic peaks at 3.68 (TC3) and 4.19 min (TC4), which had the same precursor ions $m/z$ 540.2, indicating that adduct isomers could also be detected. TC3 and TC4 were determined by three MRM transitions (540.2 → 130.0, 540.2 → 162.0, 540.2 → 164.0), corresponding to isomeric NAC adducts of oxidized triptolide. The elemental compositions of TC3 ($m/z$ 540.1884) and TC4 ($m/z$ 540.1877) were determined to be $C_{25}H_{33}NO_{10}S$ by accurate mass measurement using Q-TOF-MS/MS. The fragment ions producing from the neutral loss of NAC (−163.0 Da) and $H_2O$, and the

**Table 2**
Prediction and detection of cysteine adducts for representative compounds.

| Compounds | NAC adducts | Proposed NAC adducts | Adducts formula | Calculated $m/z$ [M + H]$^+$ | Retention time (min) | MRM | | | Observed accurate $m/z$ [M + H]$^+$ | Mass accuracy (ppm) |
|---|---|---|---|---|---|---|---|---|---|---|
| | | | | | | 130.0 | 162.0 | 164.0 | | |
| Triptolide | TC1 | TP + NAC | $C_{25}H_{33}NO_9S$ | 524.1949 | 4.49 | √ | √ | √ | 524.1954 | −0.95 |
| | TC2 | TP−2H + NAC | $C_{25}H_{31}NO_9S$ | 522.1792 | 5.96 | √ | − | √ | 522.1791 | 0.19 |
| | TC3 | TP + O + NAC | $C_{25}H_{33}NO_{10}S$ | 540.1898 | 3.68 | √ | √ | √ | 540.1907 | −1.67 |
| | TC4 | TP +O + NAC | $C_{25}H_{33}NO_{10}S$ | 540.1898 | 4.19 | √ | √ | √ | 540.1902 | −0.74 |
| | TC5 | TP−H$_2$O + NAC | $C_{25}H_{31}NO_8S$ | 506.1843 | 5.10 | √ | √ | √ | 506.1837 | 1.19 |
| Osimertinib | AC1 | AZD + NAC | $C_{33}H_{42}N_8O_5S$ | 663.3072 | 4.95 | √ | √ | √ | 663.3072 | 0.00 |
| | AC2 | AZD + O + NAC | $C_{33}H_{42}N_8O_6S$ | 679.3021 | 3.91 | √ | √ | − | 679.3004 | 2.50 |
| | AC3 | AZD + O + NAC | $C_{33}H_{42}N_8O_6S$ | 679.3021 | 4.36 | √ | √ | − | 679.3009 | 1.77 |
| | AC4 | AZD−CH$_3$ + NAC | $C_{32}H_{40}N_8O_5S$ | 649.2915 | 4.89 | √ | √ | − | 649.2913 | 0.31 |
| Naringenin | NC1 | NAR + O + NAC−2H | $C_{20}H_{19}NO_9S$ | 450.0853 | 4.93 | − | √ | − | 450.0850 | 0.67 |
| | NC2 | NAR + O + NAC−2H | $C_{20}H_{19}NO_9S$ | 450.0853 | 5.71 | √ | √ | − | 450.0852 | 0.22 |
| | NC3[a] | NAR + O−2H + NAC−2H | $C_{20}H_{17}NO_9S$ | 448.0697 | 5.53 | √ | √ | − | 448.0693 | 0.89 |

√: Detected; −: Not detected.
TP: triptolide; NAC: *N*-acetyl cysteine; AZD: osimertinib; NAR: naringenin; TC: NAC adduct of triptolide or its metabolites; AC: NAC adduct of osimertinib or its metabolites; NC: NAC adduct of naringenin or its metabolites.
[a] Represented new modification pattern.

characteristic fragment ions of NAC at $m/z$ 130.0499 and 162.0221, confirmed that NAC was added to the oxidized triptolide (Fig. S2C). In addition, TC5 with precursor ion $m/z$ 506.2 was determined by three MRM transitions (506.2 → 130.0, 506.2 → 162.0, 506.2 → 164.0), and tentatively assigned as dehydrated triptolide-NAC adduct. In the Q-TOF-MS/MS spectra, the protonated molecular ions at $m/z$ 506.1837 with the chemical formula of $C_{25}H_{31}NO_8S$, and the fragment ions from the neutral loss of $C_5H_7NO_3$ ($m/z$ 377.1388) and NAC ($m/z$ 343.1524), and characteristic NAC fragment ions at $m/z$ 130.0491, 162.0214, and 164.0365 further confirmed that TC5 was a NAC adduct of dehydrated triptolide (Fig. S2D). The four predicted NAC adducts and their related isomers were successfully detected by MRM scanning.

Osimertinib incorporates the α,β-unsaturated carbonyl warhead. The oxidized metabolite and demethylated metabolite retaining α,β-unsaturated carbonyl were acquired from the BioTransformer, and their NAC conjugates were predicted and shown in Table 2. MRM analysis showed four peaks, AC1−AC4 (Table 2, and Fig. 2B). The peak with precursor ion $m/z$ 663.3 (AC1) was determined by three MRM transitions (663.3 → 130.0, 663.3 → 162.0, 663.3 → 164.0) corresponding to osimertinib-NAC adduct. Two peaks with the precursor ion $m/z$ 679.3 (AC2 and AC3) corresponding to oxidized metabolite-NAC adducts, were determined by two MRM transitions (679.3 → 130.0, 679.3 → 162.0). The peak with precursor ion $m/z$ 649.3 (AC4), determined by two MRM transitions (649.3 → 130.0, 649.3 → 162.0), was tentatively assigned as demethylated metabolite-NAC adduct. In the Q-TOF-MS/MS spectra, the accurate mass and the fragment ions generated from the neutral loss of $C_5H_7NO_3$ (−129.0 Da) together with characteristic NAC fragment ions at $m/z$ 130.05 and 162.02, confirmed the structure of these NAC adducts (Fig. S3). The postulated NAC adducts of osimertinib and its metabolites were successfully detected.

Phenol-containing naringenin was further applied to evaluate the applicability of this strategy. The hydroxylated metabolites of naringenin were acquired from BioTransformer and the hydroxylated and dehydrogenated metabolites of naringenin have been determined in microsomal incubation system [30]. All of them were expected to be biotransformed into a reactive quinone intermediate to conjugate with NAC through Michael addition reaction (Fig. S1, and Table 2). In this study, three potential adducts, NC1−NC3, were detected by MRM scanning (Table 2, and Fig. 2C). The peaks with precursor ion $m/z$ 450.1 eluted at 4.93 min (NC1) and 5.71 min (NC2) were determined by two MRM transitions (450.1 → 130.0, 450.1 → 162.0), and were expected as NAC adducts of mono-hydroxylated metabolites of naringenin. Another peak with
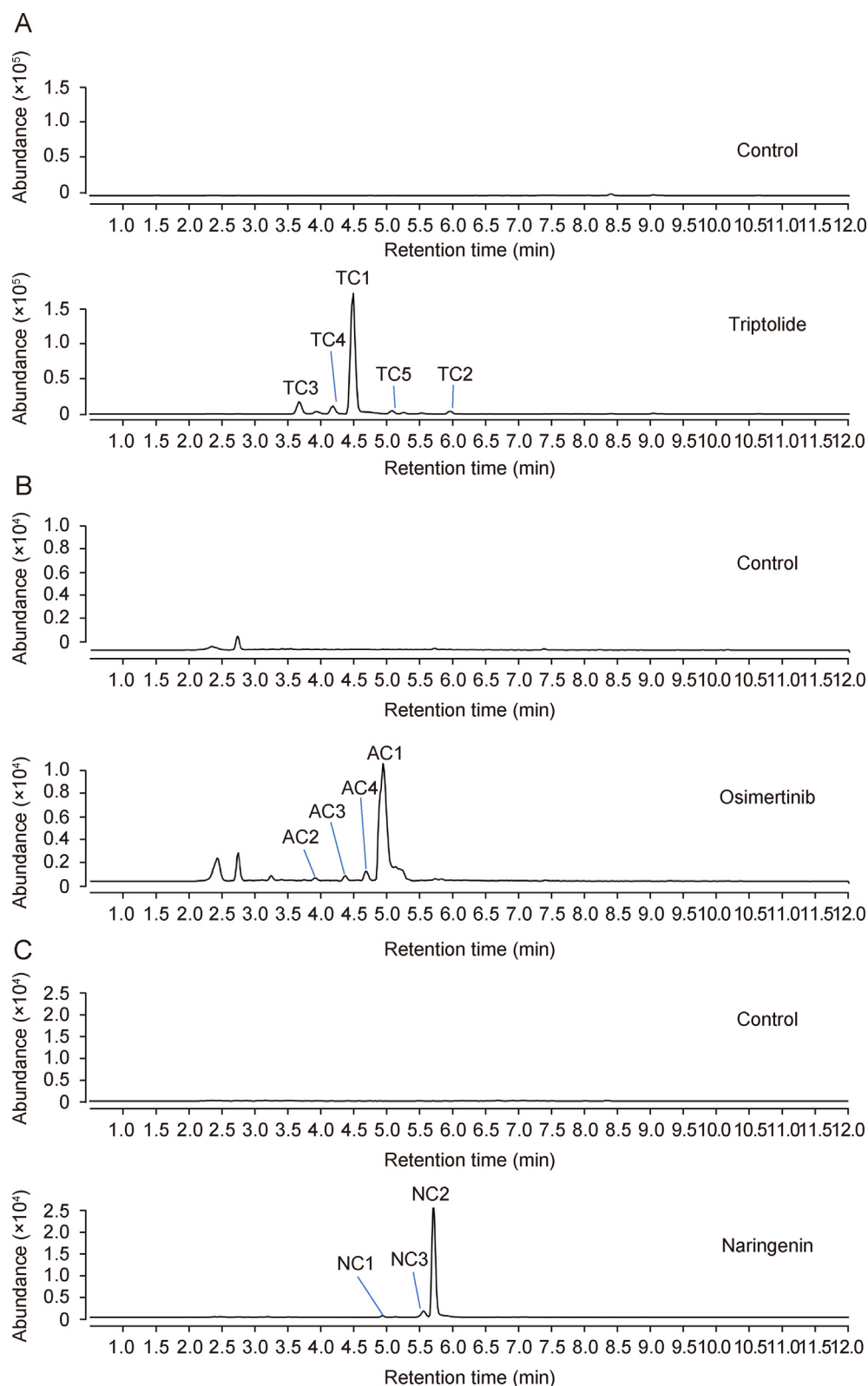
precursor ion $m/z$ 448.1 (NC3) determined by two MRM transitions (448.1 → 130.0, 448.1 → 162.0) was speculated to be a NAC adduct formed by monooxygenation and dehydrogenation of naringenin. The structures of these adducts were further verified by the accurate masses and the fragment ions produced from the loss of 129.0 Da and the characteristic fragment ions of NAC in the Q-TOF-MS/MS spectra (Fig. S4).

To ensure maximal detection sensitivity, we further optimized the collision energy in increments of 5 V from 10 to 50 V, and the optimized CE value was determined according to the highest MRM response. The results showed that the optimal collision energy for each transition varied in the range of 30 ± 5V, so it was set at 30 V to ensure sensitive monitoring of diverse potential NAC adducts. However, we found that there were a few peaks in the chromatograms of the control samples supplemented with NAC without test compound. These peaks were postulated to be formed by the reaction of NAC and endogenous components in the liver microsomes. To reduce matrix interference, we further refined the criteria for MRM analysis: (1) S/N > 3; (2) the absolute height ≥500 counts.

The successful detection for the NAC adducts of above representative compounds indicated that the product ions at $m/z$ 130.0, 162.0, and 164.0 could achieve unbiased detection of NAC adducts regardless of substrate type, warhead type, and NAC conjugate structure. The peaks of NAC adducts were confirmed with more than one MRM transition. Moreover, this strategy enables simultaneous detection and characterization of NAC adducts. And metabolites that are capable of covalently binding with NAC can be screened out, even if their prodrugs do not exhibit covalent binding properties, facilitating the exploration of potential covalent compounds. Overall, this experimental-based strategy was valuable for screening cysteine-targeting compounds from complex incubation system, independent of substrate structures, potentially shortening the time and effort in finding covalent compounds.

### 3.3. Comparison with neutral loss scan and precursor ion scan

To further evaluate the sensitivity of this strategy, neutral loss and precursor ion scan methods were also performed for comparison. Neutral loss scan is regarded as a common practice method for globally profiling unknown metabolites containing similar substructure [31]. In this research, neutral loss scanning of 129.0 Da and 163.0 Da were carried out to discover NAC adducts by QQQ-MS in the positive mode. However, only one NAC adduct of triptolide (AC1) was detected in this mode (Fig. S5A). Moreover, the peak of

**Fig. 2.** Total ion chromatograms of *N*-acetyl-cysteine (NAC) adducts formed in the microsomes incubation system with or without the substrates by multiple reaction monitoring (MRM) analysis. (A) Triptolide, (B) osimertinib, and (C) naringenin. TC: NAC adduct of triptolide or its metabolites; AC: NAC adduct of osimertinib or its metabolites; NC: NAC adduct of naringenin or its metabolites.

NAC adduct could not be easily distinguished because of the interference of large number of intense false peaks. Precursor ion scanning is another powerful method in the analysis of unknown metabolites which possess identical moieties and similar fragmentation pattern using LC-MS/MS [31,32]. The precursor ion scan was carried out for NAC adducts screening by monitoring the characteristic product ions of $m/z$ 130.0, 162.0, and 164.0 in the positive mode. However, only two potential NAC adducts of triptolide (TC1 and TC2) were detected in this mode (Fig. S5B). And the total ion chromatograms were complicated with a high background.

Most NAC adducts detected by MRM-based analysis were missed by neutral loss scan and precursor ion scan. Furthermore, the MRM-profiling of these incubation samples displayed intense NAC adducts peaks that were readily identifiable, whereas the neutral loss scan or precursor ion scan showed relatively minor chromatographic peaks and a few false peaks, resulting in NAC adducts not being immediately recognized. These results suggested that MRM-based analysis had superior sensitivity and selectivity

compared with neutral loss scan and precursor ion scan. Overall, this strategy was sensitive and effective that allowed us to quickly identify potential cysteine-targeting covalent inhibitors.

### 3.4. Potential cysteine-targeting covalent inhibitors screening

To discover potential new cysteine-targeting covalent inhibitors, the already-available drugs containing potentially electrophilic functional groups of phenyl, hexanone, quinone methides, and α,β-unsaturated carbonyls, such as ketamine, resibufogenin, celastrol, ibrutinib, sunitinib, ciprofloxacin, and ozenoxacin, were selected for screening (Table 1). The NAC adducts database was established based on the literature, online databases and covalent binding mechanisms (Table 3). The *in vitro* incubation samples were analyzed using validated strategy described above.

Ketamine possesses two potential warheads, phenyl and a hexanone, and its *S*-enantiomer, esketamine, has been approved by FDA for adult patients with treatment-resistant depression in 2019 [33]. Based on its structure, phenyl may be biotransformed to

**Table 3**
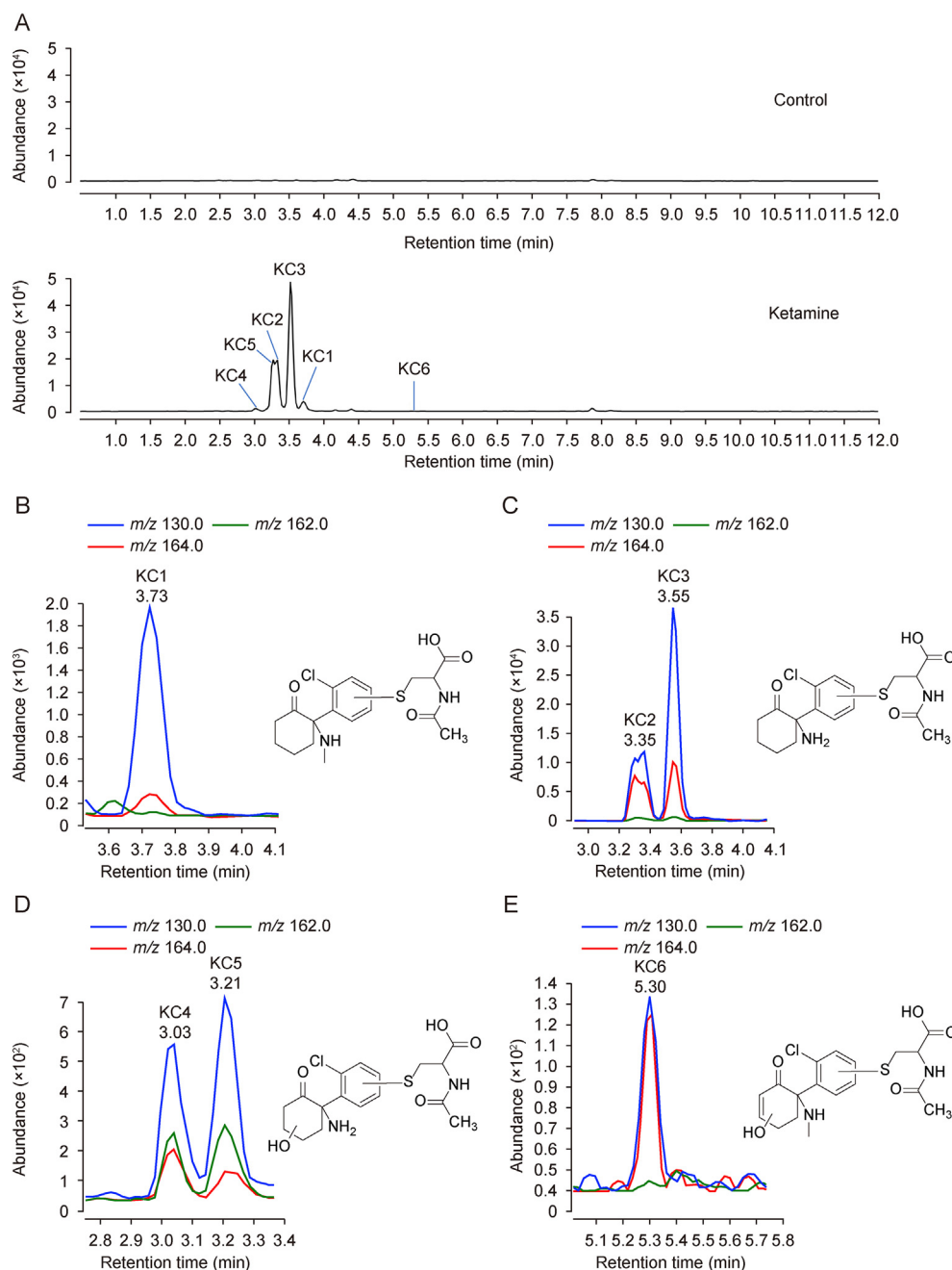Prediction and detection of cysteine adducts for screening compounds.

| Compounds | NAC adducts | Proposed NAC adducts | Adducts formula | Calculated $m/z$ [M + H]$^+$ | Retention time (min) | MRM 130.0 | 162.0 | 164.0 |
|---|---|---|---|---|---|---|---|---|
| Ketamine | KC1[a] | KET + NAC−2H/KET + O−H$_2$O + NAC | C$_{18}$H$_{23}$ClN$_2$O$_4$S | 399.1140 | 3.73 | √ | − | √ |
| | KC2[a] | KET−CH$_3$+NAC−2H/KET−CH$_3$ + O−H$_2$O + NAC | C$_{17}$H$_{21}$ClN$_2$O$_4$S | 385.0983 | 3.35 | √ | √ | √ |
| | KC3[a] | KET−CH$_3$ + NAC−2H/KET−CH$_3$ + O−H$_2$O + NAC | C$_{17}$H$_{21}$ClN$_2$O$_4$S | 385.0983 | 3.55 | √ | √ | √ |
| | KC4[a] | KET−CH$_3$ + O + NAC−2H/KET−CH$_3$+2O−H$_2$O + NAC | C$_{17}$H$_{21}$ClN$_2$O$_5$S | 401.0932 | 3.03 | √ | √ | √ |
| | KC5[a] | KET−CH$_3$ + O + NAC−2H/KET−CH$_3$ + 2O−H$_2$O + NAC | C$_{17}$H$_{21}$ClN$_2$O$_5$S | 401.0932 | 3.21 | √ | √ | √ |
| | KC6[a] | KET + O−2H + NAC−2H/KET + 2O−2H−H$_2$O + NAC | C$_{18}$H$_{21}$ClN$_2$O$_5$S | 413.0932 | 5.30 | √ | − | √ |
| Resibufogenin | RC1[a] | RES−2H + O−H$_2$O + NAC | C$_{29}$H$_{37}$NO$_7$S | 544.2363 | 6.80 | √ | − | √ |
| | RC2[a] | RES−2H + 2O−H$_2$O + NAC | C$_{29}$H$_{37}$NO$_8$S | 560.2313 | 6.35 | √ | √ | − |
| | RC3[a] | RES + 2O−H$_2$O + NAC | C$_{29}$H$_{39}$NO$_8$S | 562.2469 | 5.45 | √ | √ | − |
| | RC4[a] | RES + 3O−H$_2$O + NAC | C$_{29}$H$_{39}$NO$_9$S | 578.2418 | 5.98 | √ | √ | − |
| Celastrol | EC1 | CE + NAC | C$_{34}$H$_{47}$NO$_7$S | 614.3146 | 10.21 | √ | √ | − |
| | EC2[a] | CE + NAC−2H | C$_{34}$H$_{45}$NO$_7$S | 612.2989 | 7.69 | √ | √ | ✓ |
| | EC3[a] | CE + O + NAC−2H | C$_{34}$H$_{45}$NO$_8$S | 628.2939 | 6.33 | √ | √ | − |
| Ibrutinib | PC1 | PCI + NAC | C$_{30}$H$_{33}$N$_7$O$_5$S | 604.2337 | 7.15 | √ | √ | − |
| | PC2 | PCI−2H + NAC | C$_{30}$H$_{31}$N$_7$O$_5$S | 602.2180 | 7.30 | √ | √ | − |
| | PC3[a] | PCI−2H + O + NAC | C$_{30}$H$_{31}$N$_7$O$_6$S | 618.2129 | 6.43 | √ | − | − |
| | PC4 | PCI + O + NAC | C$_{30}$H$_{33}$N$_7$O$_6$S | 620.2286 | 6.70 | √ | √ | − |
| | PC5 | PCI + 2O + NAC | C$_{30}$H$_{33}$N$_7$O$_7$S | 636.2235 | 6.25 | √ | √ | − |
| | PC6[a] | PCI + 3O + NAC | C$_{30}$H$_{33}$N$_7$O$_8$S | 652.2184 | 6.07 | √ | √ | − |
| | PC7[a] | PCI + 3O + NAC | C$_{30}$H$_{33}$N$_7$O$_8$S | 652.2184 | 6.35 | √ | √ | − |
| Sunitinib | SC1 | SU + NAC−2H | C$_{27}$H$_{34}$FN$_5$O$_5$S | 560.2337 | 4.56 | √ | − | √ |
| | SC2 | SU−F + O + NAC−2H | C$_{27}$H$_{35}$N$_5$O$_6$S | 558.2381 | 4.42 | √ | − | √ |
| | | SU + O + NAC−2H | C$_{27}$H$_{34}$FN$_5$O$_6$S | 576.2287 | − | − | − | − |
| | | SU−C$_2$H$_4$−F + O + NAC−2H | C$_{25}$H$_{31}$N$_5$O$_6$S | 530.2068 | − | − | − | − |
| | SC3 | SU + NAC | C$_{27}$H$_{36}$FN$_5$O$_5$S | 562.2494 | 4.40 | √ | − | √ |
| | SC4[a] | SU + O + NAC | C$_{27}$H$_{36}$FN$_5$O$_6$S | 578.2443 | 3.60 | √ | − | √ |
| | | SU−C$_2$H$_4$ + NAC | C$_{25}$H$_{32}$FN$_5$O$_5$S | 534.2181 | − | − | − | − |
| | | SU−C$_2$H$_4$ + O + NAC | C$_{25}$H$_{32}$FN$_5$O$_6$S | 550.2130 | − | − | − | − |
| Ciprofloxacin | | CIP + NAC−2H | C$_{22}$H$_{25}$FN$_4$O$_6$S | 493.1552 | − | − | − | − |
| | | CIP−F + O + NAC−2H | C$_{22}$H$_{26}$N$_4$O$_7$S | 491.1595 | − | − | − | − |
| | | CIP + O + NAC−2H | C$_{22}$H$_{25}$FN$_4$O$_7$S | 509.1501 | − | − | − | − |
| | | CIP−F + NAC−2H | C$_{22}$H$_{26}$N$_4$O$_6$S | 475.1646 | − | − | − | − |
| | | CIP + NAC | C$_{22}$H$_{27}$FN$_4$O$_6$S | 495.1708 | − | − | − | − |
| | | CIP−F + O + NAC | C$_{22}$H$_{28}$N$_4$O$_7$S | 493.1751 | − | − | − | − |
| | | CIP−F + NAC | C$_{22}$H$_{28}$N$_4$O$_6$S | 477.1802 | − | − | − | − |
| | | CIP + O + NAC | C$_{22}$H$_{27}$FN$_4$O$_7$S | 511.1657 | − | − | − | − |
| Ozenoxacin | | OZE + NAC−2H | C$_{26}$H$_{28}$N$_4$O$_6$S | 525.1802 | − | − | − | − |
| | | OZE + O + NAC−2H | C$_{26}$H$_{28}$N$_4$O$_7$S | 541.1751 | − | − | − | − |
| | | OZE−C$_3$H$_4$ + NAC−2H | C$_{23}$H$_{24}$N$_4$O$_6$S | 485.1489 | − | − | − | − |
| | | OZE−C$_3$H$_4$ + O + NAC−2H | C$_{23}$H$_{24}$N$_4$O$_7$S | 501.1438 | − | − | − | − |
| | | OZE + NAC | C$_{26}$H$_{30}$N$_4$O$_6$S | 527.1812 | − | − | − | − |
| | | OZE + O + NAC | C$_{26}$H$_{30}$N$_4$O$_7$S | 543.1908 | − | − | − | − |

√: Detected; −: Not detected.
NAC: *N*-acetyl cysteine; KET: ketamine; RES: resibufogenin; CE: celastrol; PCI: ibrutinib; SU: sunitinib; CIP: ciprofloxacin; OZE: ozenoxacin,KC: NAC adduct of ketamine or its metabolites; RC: NAC adduct of resibufogenin or its metabolites; EC: NAC adduct of celastrol or its metabolites; PC: NAC adduct of ibrutinib or its metabolites; SC: NAC adduct of sunitinib or its metabolites.
[a] Represented new modification patterns.

**Fig. 3.** Multiple reaction monitoring (MRM) chromatograms of N-acetyl-cysteine (NAC) adducts formed with ketamine and its metabolites. (A) Total ion chromatograms of NAC adducts formed in the microsomes incubation system with or without ketamine by MRM analysis. (B–M) MRM chromatograms of these adducts with the product ions of *m/z* 130.0, 162.0 and 164.0. (B) KC1, (C) KC2 and KC3, (D) KC4 and KC5, and (E) KC6. KC: NAC adduct of ketamine or its metabolites.

benzene oxide to covalently bind to NAC, while the hexanone group may be oxidized and hydroxylated to form an α,β-unsaturated carbonyl to covalently bind with NAC. The predicted NAC adducts are listed in Table 3. MRM analysis of the incubation samples showed six peaks, KC1–KC6 (Fig. 3). The peak with precursor ion *m/z* 399.1 at 3.73 min (KC1) was determined by two MRM transitions (399.1 → 130.0, 399.1 → 164.0), corresponding to NAC adduct of ketamine. Two peaks eluting at 3.35 (KC2) and 3.55 min (KC3) showed the same precursor ions *m/z* 385.1, which were identified as isomeric NAC adducts of *N*-demethylated metabolites (norketamine (NK)) by three MRM transitions (385.1 → 130.0, 385.1 → 162.0, 385.1 → 164.0). Another two peaks at 3.03 min (KC4) and 3.21 min (KC5) with the same precursor ions *m/z* 401.1

were determined by three MRM transitions (401.1 → 130.0, 401.1 → 162.0, 401.1 → 164.0), and characterized as isomeric NAC adducts of hydroxylated metabolite of NK (hydroxynorketamine (HNK)). The peak at 5.30 min with precursor ions *m/z* 413.1 corresponding to a NAC adduct of oxidation and dehydrogenation metabolites (KC6), was identified by two MRM transitions (413.1 → 130.0, 413.1 → 164.0). This is the first report that reactive metabolites of ketamine could covalently bind to cysteine (Fig. S6). Moreover, they all have the potential to be developed as covalent inhibitors for the treatment of depression.

To further explore the practicality and scope of this strategy, resbufogenin was investigated. Four potential NAC adducts were predicted, as shown in Table 3. All of them were detected by MRM

scanning (Fig. S7A). The precursor ion of the peak eluting at 6.80 min was $m/z$ 544.2, corresponding to a NAC adduct of dehydrogenation metabolite of resbufogenin, which should be formed by oxidative and dehydration to an α,β-unsaturated carbonyl intermediate to react with NAC (RC1). And the peaks eluting at 6.35, 5.45, and 5.98 min showed the precursor ions at $m/z$ 560.2, 562.2, and 578.2, respectively, corresponding to NAC adducts formed with dehydrogenation and oxygenation metabolite (RC2), di-oxidation metabolite (RC3), and tri-oxidation metabolite (RC4), respectively (Fig. S8). NAC adducts formed with the metabolites containing electrophilic group after bioactivation were detected, indicating that this strategy could effectively evaluate the effects of potential compound targeting cysteine. Therefore, this strategy can be a useful tool to rapidly assess the covalent reactivity of compounds towards cysteine at the early screening stage of covalent drug development.

In addition, covalent drugs inevitably undergo metabolism during clinical application. Considering that some metabolites have the potential to exhibit better activity or pharmacokinetic characters than prodrugs, the investigation of metabolite modifications should not be neglected. Celastrol and ibrutinib were selected to investigate whether their metabolites have the potential to be developed as covalent inhibitors. Celastrol contains a para-quinone methide group that could react with cysteine residues of protein [34]. However, the low aqueous solubility of celastrol greatly limits its bioavailability [35]. Except for the previously reported adduct (EC1), two potential adducts, EC2 and EC3, formed by the addition of NAC to the quinone methide group of celastrol and its mono-oxygenated metabolite with elimination of 2H atoms, respectively, were predicted (Table 3). After MRM screening of the incubation sample, three predicted NAC adducts (EC1, EC2, EC3) were detected at 10.21, 7.69, and 7.69 min (Fig. S9). The mono-oxygenated metabolite, the substrate of EC3, has better solubility than celastrol and is expected to be developed as a promising covalent inhibitor to overcome the challenges of poor bioavailability of prodrug. Ibrutinib covalently binds to the cysteine residue in the active site of BTK via α,β-unsaturated carbonyl group [17]. In this study, seven peaks were detected (Fig. S7C). The peaks eluting at 7.15, 7.30, 6.43, 6.70, 6.25, 6.07, 6.25, and 6.07 min had the precursor ions at $m/z$ 604.2, 602.2, 618.2, 620.2, 636.2, 652.2 and 652.2, respectively, and were determined as NAC adducts of ibrutinib (PC1), dehydrogenation metabolite (PC2), dehydrogenation and oxygenation metabolite (PC3), monooxygenation metabolite (PC4), di-oxidation metabolite (PC5), and tri-oxidation metabolites of ibrutinib (PC6 and PC7) (Fig. S10). The determination of metabolites provides valuable guidance for optimizing the potency and selectivity of covalent inhibitor candidates by structure-based design.
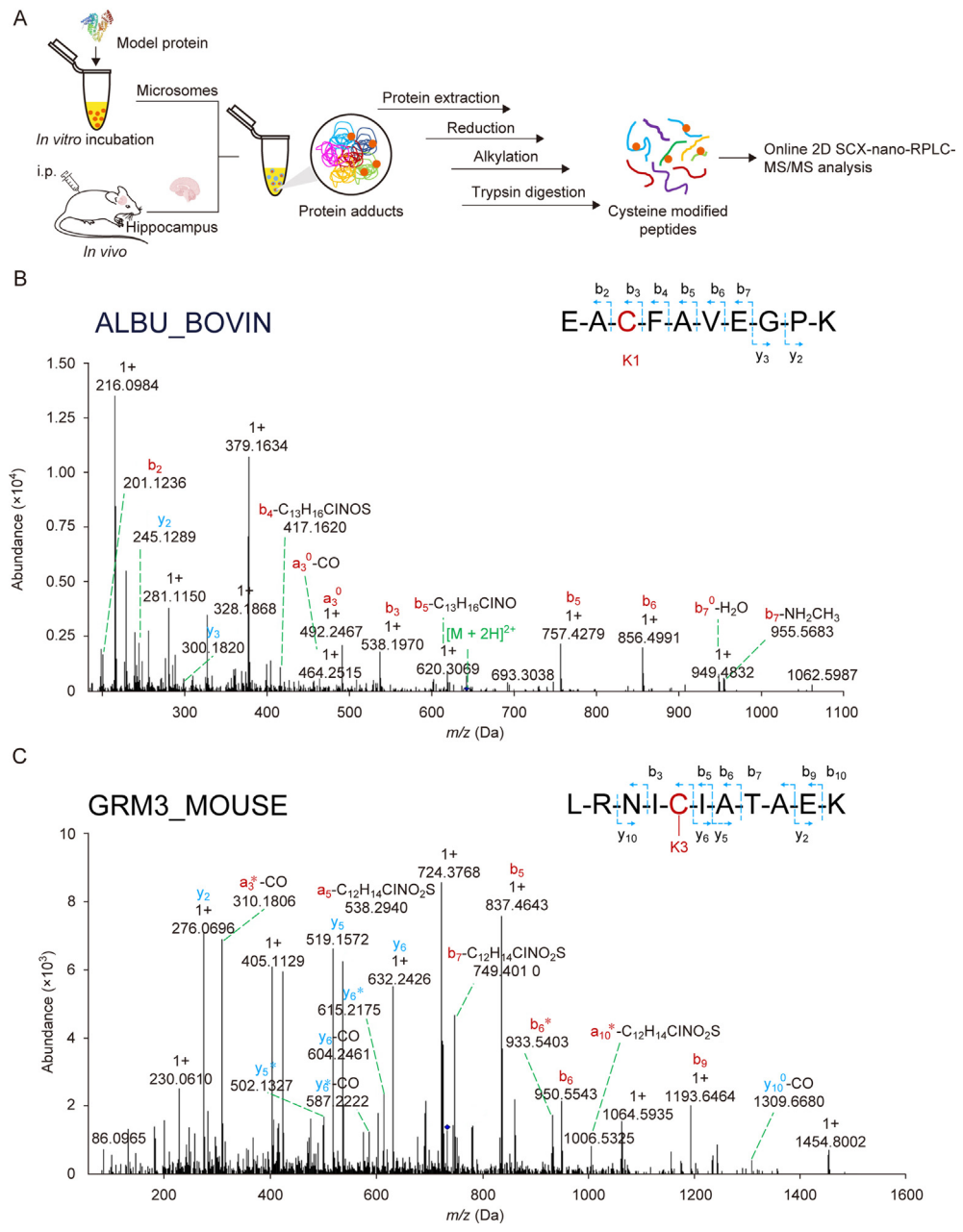
Moreover, certain drug contains more than one different type of warheads, which may exhibit different reactivity toward cysteine. To further assess the applicability of this strategy toward more elaborated compounds, sunitinib, ciprofloxacin, and ozenoxacin, which all contain two potential reactive electrophilic groups, were investigated using this strategy. Sunitinib, contains two potential warheads, phenyl and α,β-unsaturated carbonyls. Sunitinib can covalently bind to glutathione (GSH) either by bioactivation of phenyl via P450 enzymes to form an epoxide intermediate or a reactive quinoneimine [36], or by Michael addition with α,β-unsaturated carbonyl group [37]. Using our developed method, four potential NAC adducts were detected (Table 3). The peak eluting at 4.56 min showed the precursor ion of $m/z$ 560.2, corresponding to a NAC adduct formed with sunitinib epoxide intermediate (SC1). The precursor ion of $m/z$ 558.2 eluting at 4.42 min corresponded to a NAC adduct of defluorinated metabolite of sunitinib, formed by a reactive quinoneimine intermediate (SC2, Fig. S11). In addition, the peaks eluting at 4.40 min (SC3) and 3.60 min (SC4) had the

precursor ion of $m/z$ 562.2 and 578.2, respectively, corresponding to NAC adducts formed by the reaction of α,β-unsaturated carbonyl group of sunitinib and its mono-oxidation metabolite with NAC (Fig. S12). The successful detection of adducts formed by sunitinib metabolites via different electrophilic reactive groups demonstrated that this strategy could assess the reactivity of substate with multiple potential reactive groups. In addition, both ciprofloxacin and ozenoxacin contain two potential reactive electrophilic groups, phenyl and α,β-unsaturated carbonyl. They were postulated to be biotransformed into benzene oxide to covalently bind to NAC, or covalently attached to NAC with α,β-unsaturated carbonyl group. However, no potential NAC adducts were determined by MRM scanning, suggesting that ciprofloxacin, ozenoxacin, and their metabolites have no or low reaction activity with NAC (Table 3). Above results suggested that the MRM-based strategy could be applied to screen cysteine-targeting compounds in the early stage of covalent inhibitors development.

This experiment-based strategy can evaluate the reactivity of potential warheads when present in different molecular structures, thereby enabling the rapid and efficient exclusion of unreactive substrates. Using this strategy, many novel cysteine-targeting compounds or metabolites were identified and characterized, such as ketamine and resbufogenin, providing candidates for the discovery of covalent inhibitors. In addition, this screen yielded a variety of cysteine-targeting metabolites, offering structural resources for the follow-up development and design of structure-based covalent inhibitors. Moreover, structural design and optimization of potentially covalent compounds can be guided by this strategy to evaluate the reactivity of warheads. Notably, considering that large-molecule proteins with multiple binding sites and intricate three-dimensional structures could influence the kinetics and affinity of covalent interactions, the reactivity of identified promising covalent inhibitor candidates towards proteins should be further validated at the protein level. Additionally, owing to the potential risk concerns arising from irreversible covalent reaction, biological evaluation of potent and selective of promising covalent inhibitor candidates *in vivo* will be required.

### 3.5. Ketamine covalently binds to protein after bioactivation

We further evaluated whether the potential covalent inhibitor candidate could target cysteine residues of proteins (Fig. 4A). The protein adducts formed with ketamine reactive metabolites were first detected using a model protein, BSA. Ketamine was incubated with BSA in the NADPH-supplied microsomes system, followed by trypsin digestion. Online 2D SCX-nano-LC-MS/MS approach was applied to detect the modified proteins. The acquired MS and MS/MS data were searched in Mascot for the identification of modified peptides, in which the four cysteine-targeting modification patterns determined using the strategy developed above were added as variable modifications, denoted as ketamine (K1), NK (K2), HNK (K3), and oxidized and dehydrogenated ketamine (K4), respectively. The modified peptide [588]EACFAVEGPK[597] gave the molecular ion of $[M + 2H]^{2+}$ at $m/z$ 643.2825, which was increased by 178 Da compared to that of the carbamidomethyl (57 Da)-modified peptide (Fig. 4B, and Fig.S13). The fragment ion of b3 was also observed to be 178 Da heavier than that of the carbamidomethyl-modified peptide, indicating that cysteine at position 590 should be modified by K1. In addition, other fragmentation ions of b4−b7 further confirmed the modification and binding site. Moreover, Cys125 and Cys484 on BSA were also modified by K1 and K4, respectively (Fig. S14). We confirmed that ketamine or its metabolites after metabolic activation indeed can covalently attach to the cysteine residues in protein and have the potential to be developed as covalent inhibitors.

**Fig. 4.** Proteomic strategy and identification of protein adducts formed with ketamine metabolites. (A) Schematic of the experimental workflow for protein adducts detection *in vitro* and *in vivo*. (B) Tandem mass spectrometry (MS/MS) of ketamine metabolites-adducted peptides of EACFAVEGPK in bovine serum albumin (BSA). (C) MS/MS spectrum of ketamine metabolites-adducted peptides from metabotropic glutamate receptor 3 (GRM3).
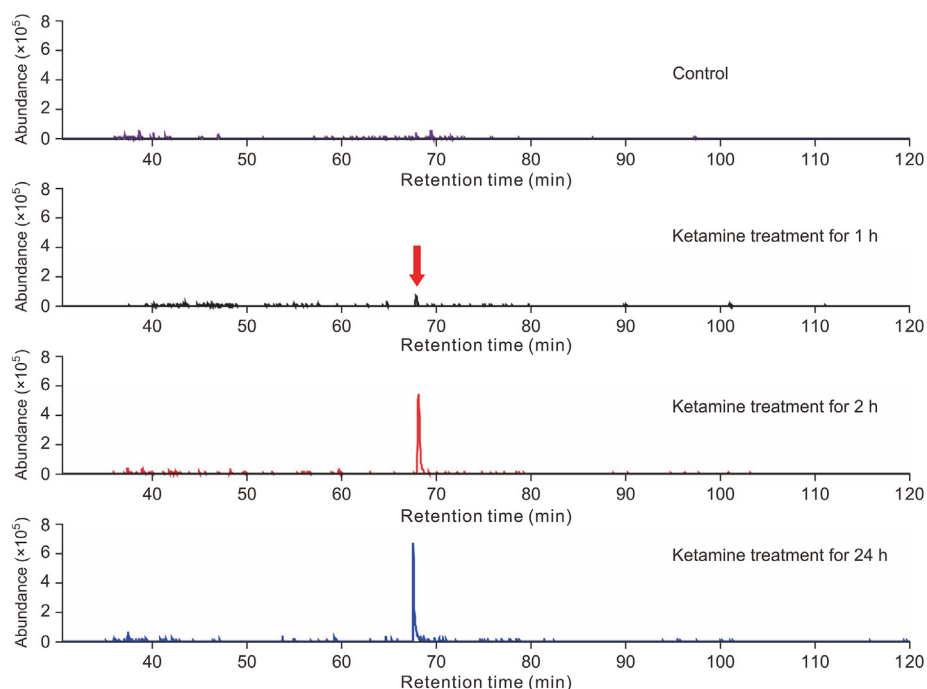
### 3.6. Novel potential covalent inhibitors discovery and target identification

It has been reported that about 20%−30% of patients with major depressive disorder develops treatment-resistant depression and finding new effective treatments for treatment-resistant depression remains a challenge [38]. Covalent inhibitors have been proved to be effective for chronic treatment of serious diseases because of the high potency and prolonged duration time [1], suggesting that covalent inhibitors have the potential advantages in the treatment

**Table 4**
Ketamine metabolites covalently modified proteins in mouse hippocampus.

| Protein | Gene | Full name | Sequence positions | Modified peptide | Observed m/z (charge) | ppm | Binding site | Modification type |
|---------|------|-----------|--------------------|------------------|-----------------------|-----|--------------|-------------------|
| GRM3 | Grm3 | Metabotropic glutamate receptor | 236−246 | LRNICIATAEK | 734.8549, 2+ | −24.46 | C240 | K3 |
| GNAZ | Gnaz | Guanine nucleotide-binding protein G(z) subunit alpha | 282−292 | IPLSVCFPEYK | 758.8711, 2+ | 2.51 | C287 | K2 |
| NCDN | Ncdn | Neurochondrin | 351−361 | CEQSLLKEPQK | 770.3779, 2+ | 13.39 | C351 | K3 |
| OGA | Oga | Protein O-GlcNAcase | 859−869 | SMMACLLSSLK | 479.5561, 3+ | 10.38 | C863 | K3 |

**Fig. 5.** Extraction ion chromatograms of metabotropic glutamate receptor 3 (GRM3) in ketamine-treated mouse hippocampus.

of treatment-resistant depression. Since the above results demonstrated that ketamine and its metabolites could covalently bind to model protein, these modification patterns seem promising to be developed as covalent inhibitors against depression. Therefore, we further investigated whether ketamine and its metabolites could covalently modify proteins *in vivo* and has the potential to be developed as novel covalent inhibitors for antidepressant.

The ketamine and its metabolites-modified proteins in the mouse hippocampus were determined using 2D SCX-nano-LC-Q-TOF MS/MS-based shotgun proteome approach. As a result, four proteins, including metabotropic glutamate receptor (GRM3), guanine nucleotide-binding protein G(z) subunit alpha (GNAZ), neurochondrin (NCDN), and protein *O*-GlcNAcase (OGA), were found to be modified in the hippocampus of mouse administered with ketamine for 1, 2, and 24 h (Table 4, and Figs. 4C and S15). The covalent modification might alter protein functions and inactivate proteins enzymatic activities [39]. GRM3 (mGlu3) was modified by a ketamine metabolite, HNK. GRM3 which regulates glutamate neurotransmission and affects synaptic plasticity, is therapeutic target for several psychiatric disorders [40,41]. The activation of mGlu3 could induce long-term depression in the mouse medial prefrontal cortex (mPFC) *in vitro*, and mGlu3 receptor negative allosteric modulators has demonstrated antidepressant efficacy [42,43]. These indicated that covalent modification of HNK might inactivate of GRM3 to produce the antidepressant effects. In addition, the mGlu2/3 receptor antagonist had been reported to increase glutamate receptor 1 (GRIA1) expression, resulting in sustained enhancement of excitatory synaptic transmission within 24 h after a single injection, similar to the effects of ketamine [44,45]. In our research, the contents of ketamine metabolites, HNK and NK, were increased rapidly at 2 h, but they were no longer detectable at 24 h in the hippocampus after administration (Fig. S16). However, the modified GRM3 in the hippocampus was found to rapidly increase between 1 and 2 h, and the contents at 24 h was similar to that at 2 h after a single dose of ketamine treatment (Fig. 5), suggesting the formation of protein adducts would accumulate, resulting in a longer duration of effects compared to ketamine and its metabolites. Moreover, GNAZ (G proteins) related to the occurrence of depression [46] were found to

be modified by NK, which might reduce the risk of developing depressive disorders. And the contents of modified GNAZ increased along with the administration time (Fig. S17). NCDN, which has a significant influence on adult hippocampal neurogenesis, was modified by HNK. And OGA as a promising therapeutic target for Alzheimer disease was also modified by HNK, which might prevent the formation of neurofibrillary tangles and associated neurodegeneration [47]. We also observed that the adducted proteins of NCDN and OGA had longer residence time than ketamine and its metabolites in the mouse hippocampus (Fig. S17). The above-mentioned modified proteins may be potential target proteins for the antidepressant effects.

The irreversible covalent modification on synaptic transmission-related proteins, such as GRM3, GNAZ, and NCDN, may disrupt their function and inactivate their activities, leading to a long duration of action, which prolonged the duration of the resulting pharmacological effects because targets inhibition persisted after prodrug had been cleared. Interestingly, we observed that these protein targets were modified by ketamine metabolites, NK and HNK, which have been reported to exert rapid and sustained antidepressant actions without the detrimental side effects [48,49]. Therefore, NK and HNK seem to be safer alternative to the prodrug as an antidepression, and they are expected to be developed as covalent inhibitors with promising potential in the treatments of treatment-resistant depression. Moreover, these results would help to elucidate the molecular mechanism of ketamine's antidepressant and provide more information on design and development of new drugs for treatment of major depression without the side effects.

## 4. Conclusion

In this study, we develop a database-assisted LC-MS/MS strategy with high selectivity and sensitivity that enables reliable and extensive screening of NAC adducts, to a certain extent addressing some key difficulties in current covalent inhibitor discovery. This strategy can cover as many adducts as possible, including those formed from prodrugs or metabolites, based on

the comprehensive HMDB database and BioTransformer, providing wider coverage for the prediction of potential cysteine-targeting compounds. This MRM-based strategy coupled with substrate-independent product ions has broad applicability and could be performed across various of potential warheads to evaluate their potential to target cysteine when present in different molecular structures. And the identified modifications of compound or its metabolites could be developed as covalent inhibitors (e.g. NK and HNK) or used to guide for the rational design and discovery of high potency covalent inhibitors. In addition, compared with previous virtual screening and fragment-based drug discovery methods [11,14], this strategy is not limited by molecular structures of evaluated compounds, so many novel and promising covalent compounds would be discovered. Furthermore, this experiment-based strategy can achieve simultaneous detection and characterization cysteine adducts. Therefore, this strategy can be used as a complementary approach to previous methods for covalent inhibitor discovery. In conclusion, this MRM-based strategy is useful for the cysteine-targeting compounds discovery. Furthermore, this strategy can also be extended to the screening of potential covalent compounds targeting non-cysteine residues, relying on the selection of appropriate trapping reagents and corresponding characteristic product ions, while future studies on non-cysteine covalent compounds are warranted.

## CRediT authorship contribution statement

**Xiaolan Hu:** Writing − original draft, Methodology, Investigation, Formal analysis, Conceptualization. **Jian-Lin Wu:** Supervision, Conceptualization. **Quan He:** Investigation. **Zhi-Qi Xiong:** Supervision. **Na Li:** Writing − review & editing, Supervision, Funding acquisition, Conceptualization.

## Declaration of competing interest

The authors declare that there are no conflicts of interest.

## Acknowledgment

## Appendix A. Supplementary data

Supplementary data to this article can be found online at https://doi.org/10.1016/j.jpha.2024.101045.

## References

[1] J. Singh, R.C. Petter, T.A. Baillie, et al., The resurgence of covalent drugs, Nat. Rev. Drug Discov. 10 (2011) 307−317.
[2] R. Lonsdale, R.A. Ward, Structure-based design of targeted covalent inhibitors, Chem. Soc. Rev. 47 (2018) 3816−3830.
[3] D.S. Hong, M.G. Fakih, J.H. Strickler, et al., KRAS$^{G12}$C inhibition with sotorasib in advanced solid tumors, N. Engl. J. Med. 383 (2020) 1207−1217.
[4] J.A. Woyach, R.R. Furman, T. Liu, et al., Resistance mechanisms for the Bruton's tyrosine kinase inhibitor ibrutinib, N. Engl. J. Med. 370 (2014) 2286−2294.
[5] V.A. Miller, V. Hirsh, J. Cadranel, et al., Afatinib versus placebo for patients with advanced, metastatic non-small-cell lung cancer after failure of erlotinib, gefitinib, or both, and one or two lines of chemotherapy (LUX-Lung 1): A phase 2b/3 randomised trial, Lancet Oncol. 13 (2012) 528−538.
[6] J.M. Strelow, A perspective on the kinetics of covalent and irreversible inhibition, SLAS Discov. 22 (2017) 3−20.
[7] R.A. Bauer, Covalent inhibitors in drug discovery: From accidental discoveries to avoided liabilities and designed therapies, Drug Discov. Today 20 (2015) 1061−1073.
[8] D. Toledo Warshaviak, G. Golan, K.W. Borrelli, et al., Structure-based virtual screening approach for discovery of covalently bound ligands, J. Chem. Inf. Model. 54 (2014) 1941−1950.
[9] J. Lyu, S. Wang, T.E. Balius, et al., Ultra-large library docking for discovering new chemotypes, Nature 566 (2019) 224−229.
[10] A. Fischer, M. Smieško, M. Sellner, et al., Decision making in structure-based drug discovery: Visual inspection of docking results, J. Med. Chem. 64 (2021) 2489−2500.
[11] N. London, R.M. Miller, S. Krishnan, et al., Covalent docking of large libraries for the discovery of chemical probes, Nat. Chem. Biol. 10 (2014) 1066−1072.
[12] E. Resnick, A. Bradley, J. Gan, et al., Rapid covalent-probe discovery by electrophile-fragment screening, J. Am. Chem. Soc. 141 (2019) 8951−8968.
[13] M.M. McCallum, P. Nandhikonda, J.J. Temmer, et al., High-throughput identification of promiscuous inhibitors from screening libraries with the use of a thiol-containing fluorescent probe, J. Biomol. Screen. 18 (2013) 705−713.
[14] D.A. Erlanson, S.W. Fesik, R.E. Hubbard, et al., Twenty years on: The impact of fragments on drug discovery, Nat. Rev. Drug Discov. 15 (2016) 605−619.
[15] A.J. Maurais, E. Weerapana, Reactive-cysteine profiling for drug discovery, Curr. Opin. Chem. Biol. 50 (2019) 29−36.
[16] Q. Zhang, P. Luo, L. Zheng, et al., 18beta-glycyrrhetinic acid induces ROS-mediated apoptosis to ameliorate hepatic fibrosis by targeting PRDX1/2 in activated HSCs, J. Pharm. Anal. 12 (2022) 570−582.
[17] L. Boike, N.J. Henning, D.K. Nomura, Advances in covalent drug discovery, Nat. Rev. Drug Discov. 21 (2022) 881−898.
[18] S. Pushpakom, F. Iorio, P.A. Eyers, et al., Drug repurposing: Progress, challenges and recommendations, Nat. Rev. Drug Discov. 18 (2019) 41−58.
[19] S. Gong, X. Hu, S. Chen, et al., Dual roles of drug or its metabolite-protein conjugate: Cutting-edge strategy of drug discovery using shotgun proteomics, Med. Res. Rev. 42 (2022) 1704−1734.
[20] J.W.T. Yates, S. Ashton, D. Cross, et al., Irreversible inhibition of EGFR: Modeling the combined pharmacokinetic-pharmacodynamic relationship of osimertinib and its active metabolite AZ5104, Mol. Cancer Ther. 15 (2016) 2378−2387.
[21] S. Gong, Y. Zhuo, S. Chen, et al., Quantification of osimertinib and metabolite-protein modification reveals its high potency and long duration of effects on target organs, Chem. Res. Toxicol. 34 (2021) 2309−2318.
[22] Z. Li, X. Zhang, J. Liao, et al., An ultra-robust fingerprinting method for quality assessment of traditional Chinese medicine using multiple reaction monitoring mass spectrometry, J. Pharm. Anal. 11 (2021) 88−95.
[23] X. Bian, Y. Zhang, N. Li, et al., Ultrasensitive quantification of trace amines based on N-phosphorylation labeling chip 2D LC-QQQ/MS, J. Pharm. Anal. 13 (2023) 315−322.
[24] Y. Zhuo, J.-L. Wu, X. Yan, et al., Strategy for hepatotoxicity prediction induced by drug reactive metabolites using human liver microsome and online 2D-nano-LC-MS analysis, Anal. Chem. 89 (2017) 13167−13175.
[25] X. Hu, J.-L. Wu, W. Miao, et al., Covalent protein modification: An unignorable factor for bisphenol A-induced hepatotoxicity, Environ. Sci. Technol. 56 (2022) 9536−9545.
[26] A. Abdeldayem, Y.S. Raouf, S.N. Constantinescu, et al., Advances in covalent kinase inhibitors, Chem. Soc. Rev. 49 (2020) 2617−2687.
[27] T.J. Monks, M. Butterworth, S.S. Lau, The fate of benzene-oxide, Chem. Biol. Interact. 184 (2010) 201−206.
[28] Q. He, D.V. Titov, J. Li, et al., Covalent modification of a cysteine residue in the XPB subunit of the general transcription factor TFIIH through single epoxide cleavage of the transcription inhibitor triptolide, Angew. Chem. Int. Ed 54 (2015) 1859−1863.
[29] F. Du, Z. Liu, X. Li, et al., Metabolic pathways leading to detoxification of triptolide, a major active component of the herbal medicine *Tripterygium wilfordii*, J. Appl. Toxicol. 34 (2014) 878−884.
[30] Y. Bai, W. Peng, C. Yang, et al., Pharmacokinetics and metabolism of naringin and active metabolite naringenin in rats, dogs, humans, and the differences between species, Front. Pharmacol. 11 (2020), 364.
[31] K. Huang, L. Huang, R.B. van Breemen, Detection of reactive metabolites using isotope-labeled glutathione trapping and simultaneous neutral loss and precursor ion scanning with ultra-high-pressure liquid chromatography triple quadruple mass spectrometry, Anal. Chem. 87 (2015) 3646−3654.
[32] P. Liu, Y. Huang, W. Cai, et al., Profiling of thiol-containing compounds by stable isotope labeling double precursor ion scan mass spectrometry, Anal. Chem. 86 (2014) 9765−9773.
[33] J. Kim, T. Farchione, A. Potter, et al., Esketamine for treatment-resistant depression - first FDA-approved antidepressant in a new class, N. Engl. J. Med. 381 (2019) 1−4.
[34] S. Sreeramulu, S.L. Gande, M. Göbel, et al., Molecular mechanism of inhibition of the human protein complex Hsp90-Cdc37, a kinome chaperone-cochaperone, by triterpene celastrol, Angew. Chem. Int. Ed 48 (2009) 5853−5855.
[35] J. Shi, J. Li, Z. Xu, et al., Celastrol: A review of useful strategies overcoming its limitation in anticancer application, Front. Pharmacol. 11 (2020), 558741.
[36] E.A. Burnham, A.A. Abouda, J.E. Bissada, et al., Interindividual variability in cytochrome P450 3A and 1A activity influences sunitinib metabolism and bioactivation, Chem. Res. Toxicol. 35 (2022) 792−806.
[37] G.M. Amaya, R. Durandis, D.S. Bourgeois, et al., Cytochromes P450 1A2 and 3A4 catalyze the metabolic activation of sunitinib, Chem. Res. Toxicol. 31 (2018) 570−584.

[38] C. Fabbri, S. Kasper, J. Zohar, et al., Drug repositioning for treatment-resistant depression: Hypotheses from a pharmacogenomic study, Prog. Neuro-psychopharmacol Biol. Psychiatry 104 (2021), 110050.

[39] M. Ke, H. Shen, L. Wang, et al., Identification, quantification, and site locali-zation of protein posttranslational modifications *via* mass spectrometry-based proteomics, Adv. Exp. Med. Biol. 919 (2016) 345−382.

[40] R. Kandaswamy, A. McQuillin, S.I. Sharp, et al., Genetic association, mutation screening, and functional analysis of a Kozak sequence variant in the metabotropic glutamate receptor 3 gene in bipolar disorder, JAMA Psychiatry 70 (2013) 591−598.

[41] L. Lyon, J.N.C. Kew, C. Corti, et al., Altered hippocampal expression of gluta-mate receptors and transporters in GRM2 and GRM3 knockout mice, Synapse 62 (2008) 842−850.

[42] A.G. Walker, C.J. Wenthur, Z. Xiang, et al., Metabotropic glutamate receptor 3 activation is required for long-term depression in medial prefrontal cortex and fear extinction, Proc. Natl. Acad. Sci. USA 112 (2015) 1196−1201.

[43] J.L. Engers, K.A. Bollinger, R.L. Weiner, et al., Design and synthesis of *N*-aryl phenoxyethoxy pyridinones as highly selective and CNS penetrant mGlu₃ NAMs, ACS Med. Chem. Lett. 8 (2017) 925−930.

[44] H. Koike, S. Chaki, Requirement of AMPA receptor stimulation for the sus-tained antidepressant activity of ketamine and LY341495 during the forced swim test in rats, Behav. Brain Res. 271 (2014) 111−115.

[45] J.M. Dwyer, A.E. Lepack, R.S. Duman, mTOR activation is required for the an-tidepressant effects of mGluR2/3 blockade, Int. J. Neuropsychopharmacol. 15 (2012) 429−434.

[46] N.B. Senese, M.M. Rasenick, J.R. Traynor, The role of G-proteins and G-pro-tein regulating proteins in depressive disorders, Front. Pharmacol. 9 (2018), 1289.

[47] A.F. Abdel-Magid, Inhibition of O-GlcNAcase (OGA): A potential therapeutic target to treat Alzheimer's disease, ACS Med. Chem. Lett. 5 (2014) 1270−1271.

[48] C. Yang, S. Kobayashi, K. Nakao, et al., AMPA receptor activation-independent antidepressant actions of ketamine metabolite (S)-norketamine, Biol. Psy-chiatry 84 (2018) 591−600.

[49] P. Zanos, T.D. Gould, Mechanisms of ketamine action as an antidepressant, Mol. Psychiatry 23 (2018) 801−811.